Event-Feature-Based Clustering Reveals Continuous Distribution of Tectonic Tremors of 0.3–100 s: Application to Western Japan

Seiya Yano[1], **Satoshi Ide**[1]

[1]Department of Earth and Planetary Science, The University of Tokyo, Tokyo, Japan

Corresponding author: Seiya Yano (s-yano@eps.s.u-tokyo.ac.jp)

Key Points:

- We compile a more complete tectonic tremor catalog for western Japan using a clustering method based on event features.
- Event duration, newly defined using energy radiation, clearly separates tectonic tremors from fast earthquakes.
- Tectonic tremors, ranging in duration from 0.3 to 100 s, are consistent with the scaling law of slow earthquakes.

Abstract

We develop a methodology to compile an objective tremor catalog by combining the envelope cross-correlation method with clustering, utilizing distinctive event features that can differentiate tectonic tremors from non-tremor events. This approach enables tremor extraction without subjective criteria, allowing for the detection of short-duration tremors overlooked in previous studies. The event features are depth, the mean amplitudes at high and low frequencies, the ratio of these two amplitudes, and event duration, which is defined as the minimum period within which 50 % of the seismic energy is concentrated. The application of this method for western Japan detects 1.7 times more tremors compared with previous studies, with durations of 0.3 to ~100 s. The events with short durations are considered low-frequency earthquakes. The relationship between seismic moment and duration of the detected tremors adheres to the scaling law of slow earthquakes.

Plain Language Summary

Slow earthquakes are characterized by very slow underground deformation compared with regular (fast) earthquakes and are important in understanding the preparation period prior to large earthquakes. Tectonic tremors are a type of slow earthquakes. These tremors radiate tiny seismic waves with frequencies of several Hz, occur episodically and densely in space and time, and may last for long durations of up to several hundred seconds, which is much longer than the durations of fast earthquakes of equivalent magnitude. In this study, we detect tectonic tremors and differentiate them from fast earthquakes and anthropogenic events using a set of event features without relying on subjective criteria. The durations of tremors range from 0.3 to ~100 s and appear to be consistent with a previously proposed scaling relationship for slow earthquakes, which suggests that fast earthquakes and slow earthquakes have different physical mechanisms.

1 Introduction

The recent development of seismological and geodetic observation networks has led to the discovery of slow earthquakes, which include phenomena such as tectonic tremors and low-frequency earthquakes (LFEs) observed in a seismological frequency range of 1–10 Hz, very low-frequency earthquakes (VLFEs) in a frequency range of 0.02–0.05 Hz, and geodetically observed slow slip events (SSEs). The history of the discovery of these events has been summarized by Beroza and Ide (2011), and their potential relationships with large or giant earthquakes have been discussed by Obara and Kato (2016). Recent developments in

slow earthquake research have been reviewed by Nishikawa et al. (2023), and geological aspects of slow earthquakes have been reviewed by Behr and Bürgmann (2021).

Although the time scales vary by more than 6–7 orders of magnitude from LFEs (<1 s) to SSEs (>1 d), these slow earthquakes are strongly correlated both spatially and temporally, and have similar deformation mechanisms; consequently, they have been hypothesized to be different manifestations of a unified phenomenon across various frequency ranges (Ide et al., 2007). One feature that distinguishes these unified slow earthquakes from fast earthquakes is the relationship between seismic moment and duration. For slow earthquakes, a linear relationship between seismic moment and duration delineates the upper limit of slow earthquakes (Ide et al., 2007; Ide & Beroza, 2023), whereas the seismic moment of fast earthquakes is proportional to the cube of duration. In accordance with the hypothesis of a unified slow earthquake process, we may use seismically detected tremors as indicators of a longer geodetic process, as assumed in many recent studies (Aguiar et al., 2009; Bletery et al., 2017; Gomberg et al., 2016; Gombert & Hawthorne, 2023; Wech et al., 2010).

One of the most commonly employed methods to detect tremors is the envelope cross-correlation method (Ide, 2010; Obara, 2002; Wech & Creager, 2008), in which the inter-station similarity of S-wave envelopes is used to detect and locate tremors. However, this method detects all seismic events and cannot distinguish between slow and fast earthquakes. Therefore, additional selection criteria are required to compile a tremor catalog from detected candidate events. Previously adopted criteria include spatiotemporal event density (Wech & Creager, 2008), duration threshold (Mizuno & Ide, 2019), and even visual inspection (Romanet & Ide, 2019). Although these criteria rely on empirical knowledge or trial and error, better criteria may be established using more fundamental event features that differentiate slow earthquakes from fast earthquakes.

It is already known that (1) tremor depths are limited in some ranges, (2) tremors may last for seconds to minutes, (3) tremors lack high-frequency seismic wave energy, and (4) tremors tend to cluster spatiotemporally. Based on these observations, this study develops a method to compile a tremor catalog without subjective criteria by establishing a consistent framework for event detection, event feature calculation, and tremor extraction through machine learning. In this paper, we introduce the evaluation of event features and the clustering method in the Method section. We apply the evaluation and method to continuous seismic records for western Japan, one of the most intensively studied slow earthquakes

regions. The findings are given in the Result section. The tremors we detect have durations of 0.3–100 s and show a scaling law between duration and seismic energy. In the Discussion section, we consider the significance of this scaling law compared with the previously suggested relationship between duration and seismic moment. Conclusion section summarizes our study.

2 Method

We compile a tremor catalog through four steps (Figure 1). In the first step, we detect tremor candidates from continuous waveform data using the envelope cross-correlation method (Mizuno & Ide, 2019). In the second step, we compute event features for all detected candidate events. In the third step, we apply a density-based clustering algorithm to the set of event features to extract tremors. Finally, in the fourth step, to improve the completeness of the catalog, we reclassify noise events, which are not assigned to any meaningful clusters by the clustering algorithm, through supervised learning. The training data for supervised learning are prepared by removing isolated events from the established tremor clusters using the modified spatiotemporal clustering method of Zaliapin and Ben-Zion (2013).

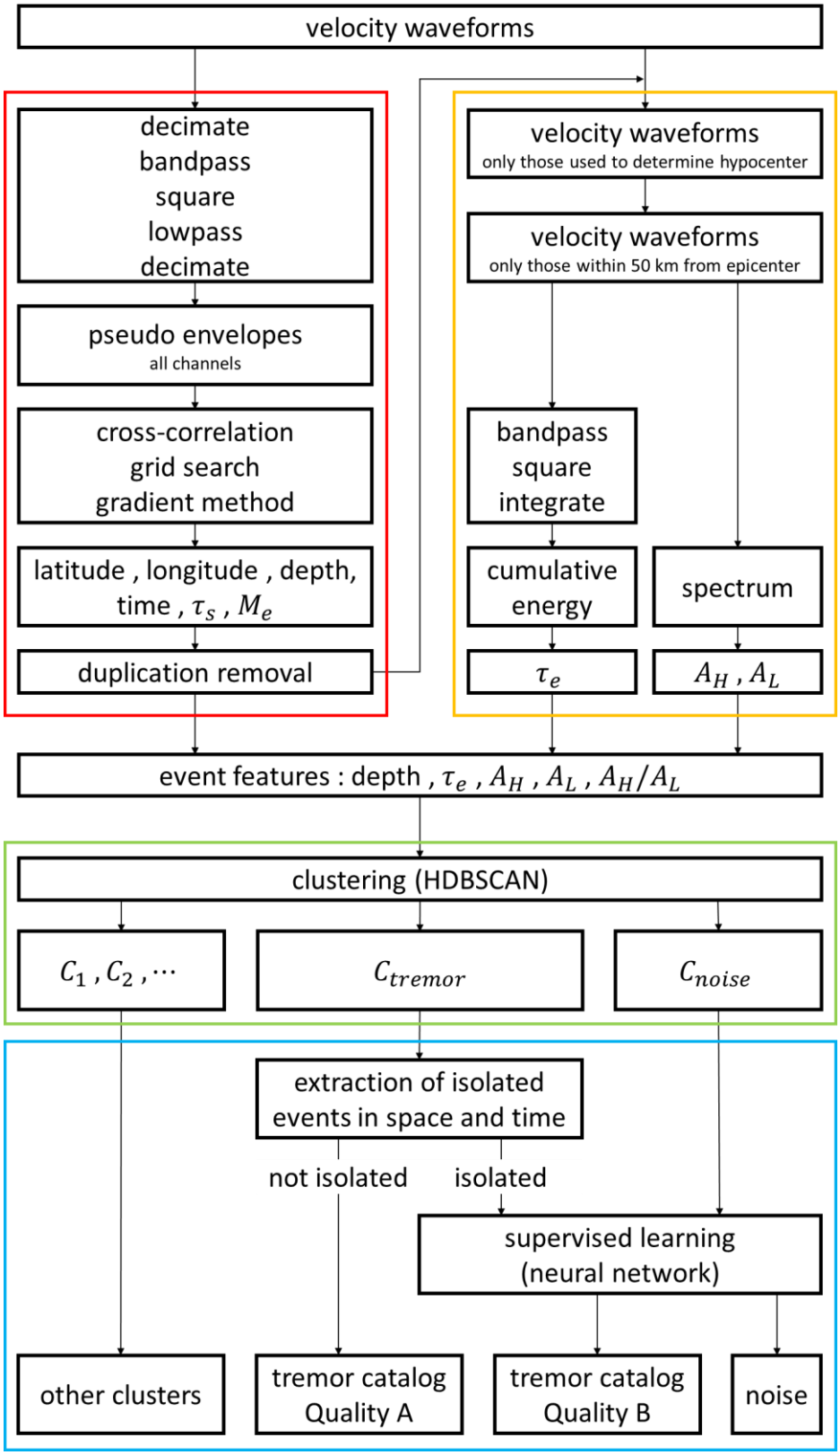

Figure 1. Flow chart of the procedure for compiling tremor catalog. The four steps explained in the text correspond to the parts surrounded by red (step 1), orange (step 2), green (step 3), and blue (step 4).

2.1 Detection of Candidate Events

We employ the method of Mizuno and Ide (2019) to detect seismic events. Those authors improved the conventional tremor detection methods (Wech & Creager, 2007, 2008) by integrating envelope cross-correlation and the maximum likelihood method, assuming that the observed envelope waveform at each seismic station results from the sum of a common envelope waveform emitted from the source and Gaussian noise. The input data are velocity seismograms resampled at 20 samples per second (sps), bandpass filtered at 2–8 Hz, squared, and resampled at 1 sps with a lowpass filter below 0.2 Hz. The square root of these data effectively approximates the envelopes.

We search for events in each half-overlapping time window, spanning 300 s and shifted by 150 s. A single time window may contain multiple events because the method considers local maxima rather than a global maximum of the likelihood function. The bootstrap method is applied to assess the error in source determination, and events with standard errors exceeding 2.0 km are excluded from further analysis. We also compute an azimuthal gap for each event from all stations used to determine the hypocenter and remove the event if the azimuthal gap exceeds 180°. Owing to the overlap of the time window, one event is often identified twice in consecutive windows. We removed such multiple detections. The result of the procedure described above is a catalog of candidate events.

The hypocentral time and size of each event are measured as follows. We backproject the waveforms at each station employed in the estimation of the hypocenter by the time-shift caused by the S-wave travel time and square the waveforms multiplied by the hypocentral distance. When multiplied by $4\pi\rho\beta$, the mean of these functions approximates the seismic energy rate, which we denote as $\dot{E}(t)$, where ρ and β are the density and S-wave velocity, respectively. The hypocentral time t_{hypo} is identified as the moment when $\dot{E}(t)$ attains its maximum. We define the stacked envelope duration τ_s as the period during which $\dot{E}(t)$ exceeds one-quarter of its maximum value, and we quantify the observed seismic energy E_s^{obs} as the integral of $\dot{E}(t)$ over the period τ_s. We also divide τ_s into τ_{pre} and τ_{pos}, representing the periods before and after the peak of $\dot{E}(t)$, respectively.

2.2 Event Features

We extract tremors by applying a clustering method to a set of features of detected candidates. One of the features is hypocentral depth, as tremor depth is known to be limited to a certain range. We introduce other features related to event duration and signal amplitudes,

as described below.

Event duration is useful in selecting tectonic tremors. However, the stacked envelope duration τ_s is usually longer than a few seconds because we measure it using the smoothed seismic wave energy rate resampled at 1 sps after lowpass filtering below 0.2 Hz. The energy rate is also the average over all stations, which may include elongated signals caused by later phases, known to be critical for estimating the duration of shallow tectonic tremors (Toh et al., 2023). Given this problem, τ_s tends to overestimate the duration of the real source process, if it is shorter than a few seconds. Therefore, we propose a new measure denoted as the minimum energy duration τ_e, which represents the shortest duration over which half the seismic energy is concentrated. For each event, each original velocity seismogram is bandpass filtered at 2–8 Hz, squared, and integrated for the period $2\tau_s$ (Figure S1 in Supporting Information). The resulting function $E_i(t)$ approximates the seismic energy measured at the i-th channel. Given $E_i(t)$, we measure the shortest period τ_i that covers half the total seismic energy at the channel. We define the minimum of $\{\tau_i\}$ as the minimum energy duration τ_e. Computational details are explained in Text S1 in Supporting Information.

As tremors usually lack high-frequency seismic energy, information about the relative amplitude between high- and low-frequency signals is also useful for selecting tremors (e.g. Nakajima & Hasegawa, 2021; Sit et al., 2012). In the present study, we define two features of the frequency domain: high-frequency amplitude A_H and low-frequency amplitude A_L. These are the representative values of the spectral amplitude of original velocity waveforms within high- and low-frequency bands, respectively. Details of the calculation are explained in Text S2 in Supporting Information.

We use depth, τ_e, A_H, A_L, and A_H/A_L as features for clustering. Each feature may have a distribution that differs markedly from a normal distribution. To facilitate the clustering, we subject all event features to the Box–Cox transformation (Box & Cox, 1964) and subsequently standardize them to achieve a mean of 0 and a variance of 1 (Text S3 in Supporting Information).

2.3 Clustering of Candidate Events

We extract tremors from the detected candidate events using HDBSCAN (Campello et al., 2013), a density-based clustering method. HDBSCAN utilizes a mutual reachability distance instead of a Euclidean distance to efficiently form clusters with disparate densities.

The algorithm constructs a minimum spanning tree and subsequently determines whether each node and following trees should be considered as parts of distinct clusters or the same cluster, based on a stability index. We need to specify only one parameter, denoted as m_{pts}, which represents the minimum number of elements required for cluster generation. The optimal value of m_{pts} can be objectively determined by assessing the density-based clustering validation (DBCV) score (Moulavi et al., 2014). The DBCV score is an index that compares the density in the sparsest region among clusters with that in the densest region among inter-cluster regions and deems a model favorable if the former surpasses the latter. In our study, we define m_{pts} as the number corresponding to p % of the total number of candidate events. The value of p is selected by varying it from 0.05 to 5.00 in increments of 0.01 and choosing the p that yields the best DBCV score.

2.4 Reclassification Using Supervised Learning

Density-based clustering algorithms tend to classify events in low-density regions as noise events that do not belong to any of the meaningful clusters. This raises the possibility of improper clustering for the end-members of tremors, such as events with very long durations. Given that the clustering algorithm yields clusters C_{tremor}, C_1, C_2, ⋯, and C_{noise}, where C_{tremor} and C_{noise} represent the tremor cluster and noise event group, respectively, we attempt to reclassify the events in C_{noise} using supervised learning to construct a more comprehensive tremor catalog.

As the outcome of supervised learning is strongly influenced by the quality of training data, it is preferable to ensure that the tremor cluster for training data does not include non-tremor events. Given that tremors tend to occur close to each other, both spatially and temporally (e.g., Obara, 2002), we remove spatiotemporally isolated events from C_{tremor} and add them to C_{noise}. We denote the clusters of tremors and the set of noise events after this change as C'_{tremor} and C'_{noise}, respectively. We designate the tremors in C'_{tremor} as "Quality A" tremors. We use C_1, C_2, ⋯, and C'_{tremor} (not C_{tremor}) for training data and reclassify the events in C'_{noise} into all the established clusters C_1, C_2, ⋯, and C'_{tremor}.

We identify isolated events using the modified nearest-neighbor clustering method of Zaliapin and Ben-Zion (2013), in which the association between seismic events in a region can be quantified by the product of spatial and temporal distances between events. Using this spatiotemporal distance, we can distinguish between isolated events following a Poisson

process and triggered events (Baiesi & Paczuski, 2004; Zaliapin et al., 2008; Zaliapin & Ben-Zion, 2013). In the present study, we modify the definition of temporal distance and define it as the time difference between events divided by event duration τ_e. The details are given in Text S4 in Supporting Information.

We employ a neural network for the supervised learning reclassification. A neural network is a multi-layered network comprising one input layer, one or multiple hidden layers, and one output layer (Figure S2 in Supporting Information). By optimizing the parameters of the hidden layers using training data, the network can transform new input data linearly or nonlinearly in the hidden layers and output the probability of the data belonging to a specific group. In this study, we first optimize the neural network using the clusters C'_{tremor}, C_1, C_2, ⋯, and then reclassify each event in C'_{noise}.

As the result of the neural network has a weak dependence on the initial values of weights, which represent the coupling strength between two neurons, we perform reclassification five times while changing the initial values. Only those events that are reclassified as tremors with a probability of more than 99 % for all five times are assigned as "Quality B" tremors. Events whose probability of belonging to the tremor cluster is less than 99 % at least once are assigned as neither Quality A nor Quality B tremors. The event information for training and reclassification includes τ_e, A_H, and A_L, with depth and A_H/A_L being excluded. Hyperparameters of the neural network, such as the number of neurons, the number of hidden layers, and activation function, are determined through the procedure explained in Text 5 in Supporting Information.

Therefore, the final tremor catalog comprises two categories of events: those in C'_{tremor} (Quality A) and those classified as tremors through the reclassification by neural network (Quality B). The former events are more reliable, and the latter events are included to improve the completeness of the tremor catalog.

3 Data

We apply the method described above to continuous seismograms recorded at 366 Hi-net stations maintained by the National Research Institute for Earth Science and Disaster Resilience in western Japan (Figure 2a and Table S1 in Supporting Information). We use two horizontal components of velocity data originally recorded at 100 sps. The analysis period covers one year (2010). The travel time is calculated based on the travel time table of the Japan Meteorological Agency (JMA) (Ueno et al., 2002).

241

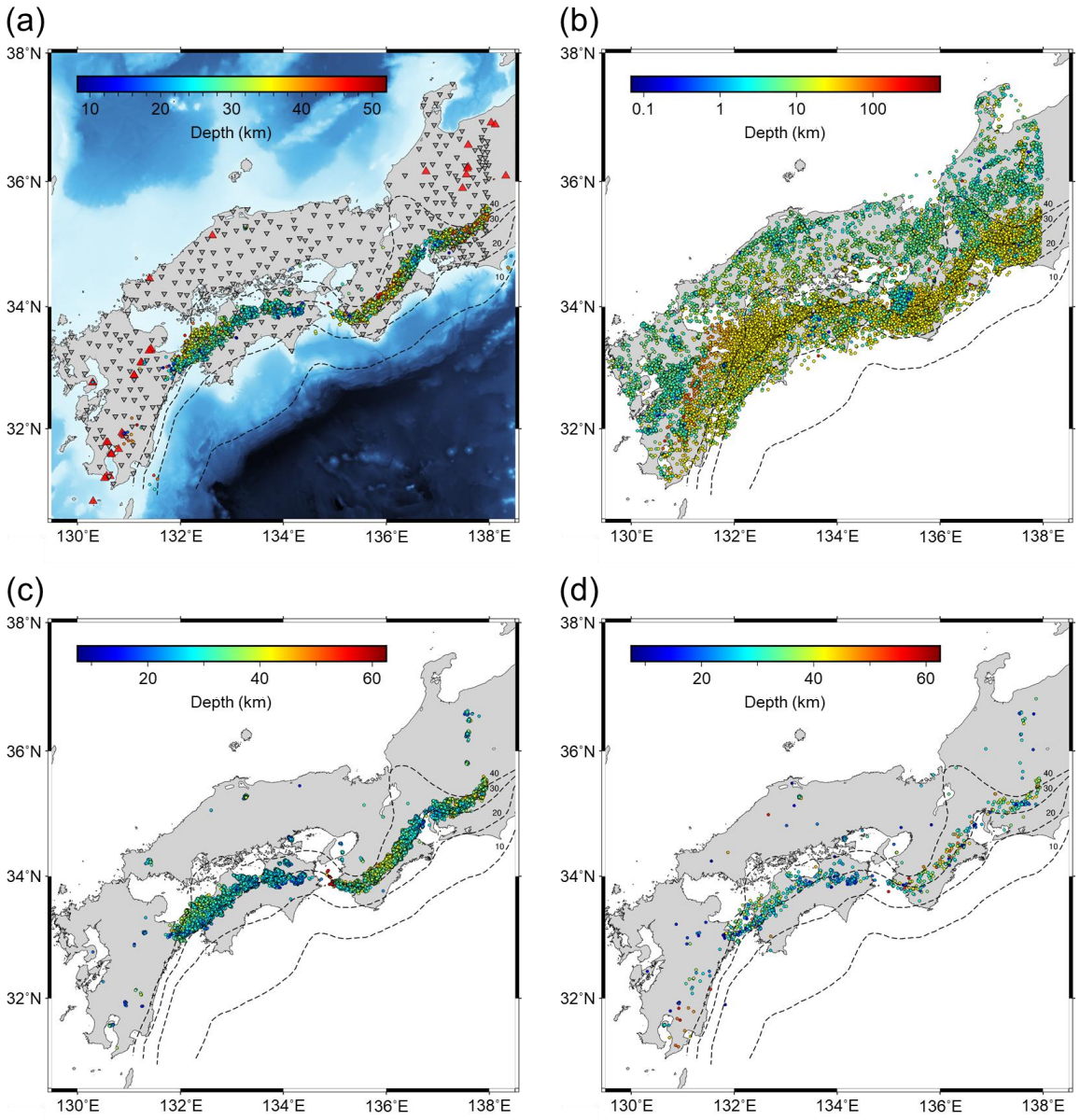

242

243 **Figure 2.** Distributions of (a) tremors detected in a previous study (Mizuno & Ide, 2019), (b)
244 all seismic events detected in this study, (c) Quality A tremors, and (d) Quality B tremors.
245 Red triangles and inversed gray triangles in (a) represent volcanoes and the Hi-net seismic
246 stations used in this study, respectively. Dashed lines are contours of the upper surface of the
247 subducting Philippine plate (Baba et al., 2002; Hirose et al., 2008; Nakajima & Hasegawa,
248 2007). Seafloor topography in (a) is based on Tozer et al. (2019).

249

250 **4 Results**

251 The envelope cross-correlation method detects 56,775 candidate events (Figure 2b).
252 The depth distribution of these events has two distinct peaks (Figure 3a). The shallow (~5

km) peak corresponds to shallow crustal earthquakes, tremors, and anthropogenic events, whereas the deep peak (~35 km) represents deep crustal earthquakes and tremors around the plate boundary. The events deeper than 60 km are intraslab earthquakes.

The minimum energy duration τ_e is shorter than the stacked envelope duration τ_s (Figure S3 in Supporting Information). τ_e has a conspicuous low-density region around $\tau_e = 0.4$ s (Figure 3b), clearly separating fast and slow earthquakes. The separation cannot be observed in τ_s (Figure 3d), as also reported in the observation of tectonic tremors in New Zealand (Romanet & Ide, 2019).

The two-dimensional density profile with A_L and A_H exhibits three distinct modes characterized by different values of A_H/A_L (Figure 3c), where we define A_H as the mean amplitude of 10–20 Hz and A_L as that of 2–8 Hz, given that the dominant frequencies for Mw 1 fast earthquakes and tremors are 10–20 Hz and 1–8 Hz, respectively (Beroza & Ide, 2011), and the influence of microseism extends up to 2 Hz (Peterson, 1993). Following the Box–Cox transformation and standardization of depth, τ_e, A_H, A_L, and A_H/A_L, the HDBSCAN algorithm identifies four meaningful clusters: $C_{shallow}$, comprising 11,795 events corresponding to fast earthquakes in the crust; C_{deep}, encompassing 2,116 events corresponding to fast earthquakes near the plate interface; C_{tremor}, comprising 24,881 events indicative of tremors; and $C_{anthropogenic}$, including 7,218 events corresponding to anthropogenic seismic events (Figure S4 in Supporting Information). HDBSCAN categorizes the remaining 10,765 events as noise events. Here, the clustering parameter m_{pts} is 34, corresponding to $p = 0.06$ %.

In the tremor cluster C_{tremor}, 1,859 events are identified as isolated events, resulting in 23,022 Quality A tremors. Subsequently, employing the neural network trained with $C_{shallow}$ (11,795 events), C_{deep} (2,116 events), C'_{tremor} (23,022 events), and $C_{anthropogenic}$ (7,218 events), we reclassify the 7,582 events that occurred at depths from 10 km to 60 km out of 12,624 events in C'_{noise}. Events in C'_{noise} with depths shallower than 10 km or deeper than 60 km are excluded before the reclassification because almost all of the events in the established four clusters occur within 10–60 km. We employ the neural network with eight neurons, two hidden layers, and the activation function $\tanh(x)$ for the reclassification, resulting in 830 Quality B tremors. Consequently, we obtain 23,022 Quality A tremors and 830 Quality B tremors (Figure 2c, d, Data Set S1 in Supporting Information).

Of 23,852 tremors (Quality A and B), 1,756 events are also listed in the JMA catalog, and 99.6 % of these events are labeled as LFE by the JMA; for the Quality A tremors, the rate

of correct classification exceeds 99.7 %. The events that are also listed in the JMA catalog tend to have a relatively large seismic energy among all tremors detected in this study. Figure S5 in Supporting Information shows an example of events classified as tremor in this study but not labeled as LFE in the JMA catalog.

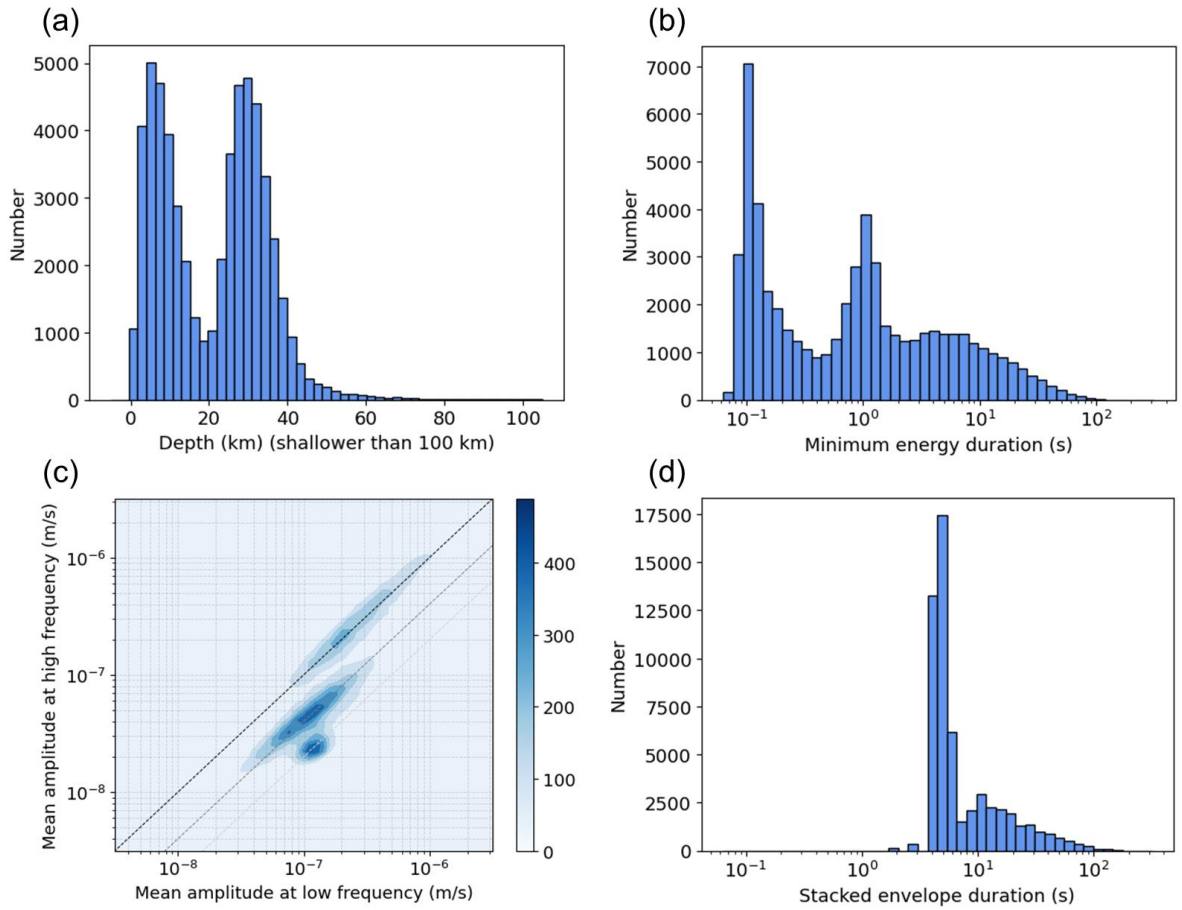

Figure 3. Distributions of (a) depth, (b) minimum energy duration τ_e, (c) low-frequency amplitude A_L and high-frequency amplitude A_H, and (d) stacked envelope duration τ_s. Dashed lines in (c) are $A_H = A_L$, $A_H = 0.4 \times A_L$, and $A_H = 0.2 \times A_L$.

5 Discussion

5.1 Duration Statistics

We detected 1.7 times more tremors compared with Mizuno and Ide (2019). This increase is due mainly to the detection of many short-duration events that were excluded in the previous study. The frequency distribution of duration in both τ_s and τ_e follows an exponential law (Figure S6 in Supporting Information). This result is consistent with previous studies (Chestler & Creager, 2017; Hiramatsu et al., 2008; Watanabe et al., 2007; Yabe & Ide,

2014), suggesting a scale limit in the tremor source (Aki & Koyanagi, 1981; Benoit et al., 2003).

5.2 Scaling Relationship

The duration of tremors in this study ranges between 0.3 to 100 s. Figure 4a compares observed seismic energy E_s^{obs} and minimum energy duration τ_e, revealing that τ_e of tremors increases almost linearly with E_s^{obs}, whereas the relationship for fast earthquakes is almost constant. However, caution is needed when interpretating the diagram as E_s^{obs} is affected by bandwidth limitation and attenuation.

For fast earthquakes, we estimate the seismic moment M_0 and event duration τ from E_s^{obs} by assuming the omega-square model and circular faults (Aki, 1967; Madariaga, 1976). Details of the calculation are described in Text S6 in Supporting Information. However, the effects of bandwidth limitation and attenuation on tremors are almost negligible owing to the low predominant frequency and its coincidence with the frequency band we used. Several previous studied have demonstrated that the scaled energy of LFEs, VLFEs, and SSEs is around 10^{-10} to 10^{-9} (Maeda & Obara, 2009; Maury et al., 2018; Yabe & Ide, 2014). Given these reports, we convert E_s^{obs} of tremors to M_0 by multiplying by $10^{-9.5}$. Figure 4b compares the estimated seismic moment and event duration. As we assume an omega-square model with constant stress drop, it is unsurprising that all fast earthquakes fall along a single straight line.

The scaling law of slow earthquakes within the time scale range of 0.5–20 s (between LFEs and VLFEs) has not been comprehensively observed or discussed. Previous studies examining a time scale of 1 s or less have produced varying conclusions, with reports suggesting that the scaling of slow earthquakes is close to $M_0 \propto \tau^3$ (Supino et al., 2020), or neither $M_0 \propto \tau^3$ nor $M_0 \propto \tau$ (Bostock et al., 2015; Farge et al., 2020). However, our results suggest that tremors follow the scaling relationship $M_0 \propto \tau$ even for events with a duration of less than 1 s. Those events with the shortest durations are impulsive and can be recognized as simple LFEs, whereas those with duration of more than several tens of seconds would include many LFEs. Therefore, our catalog contains a seamless distribution of LFEs and longer tremors.

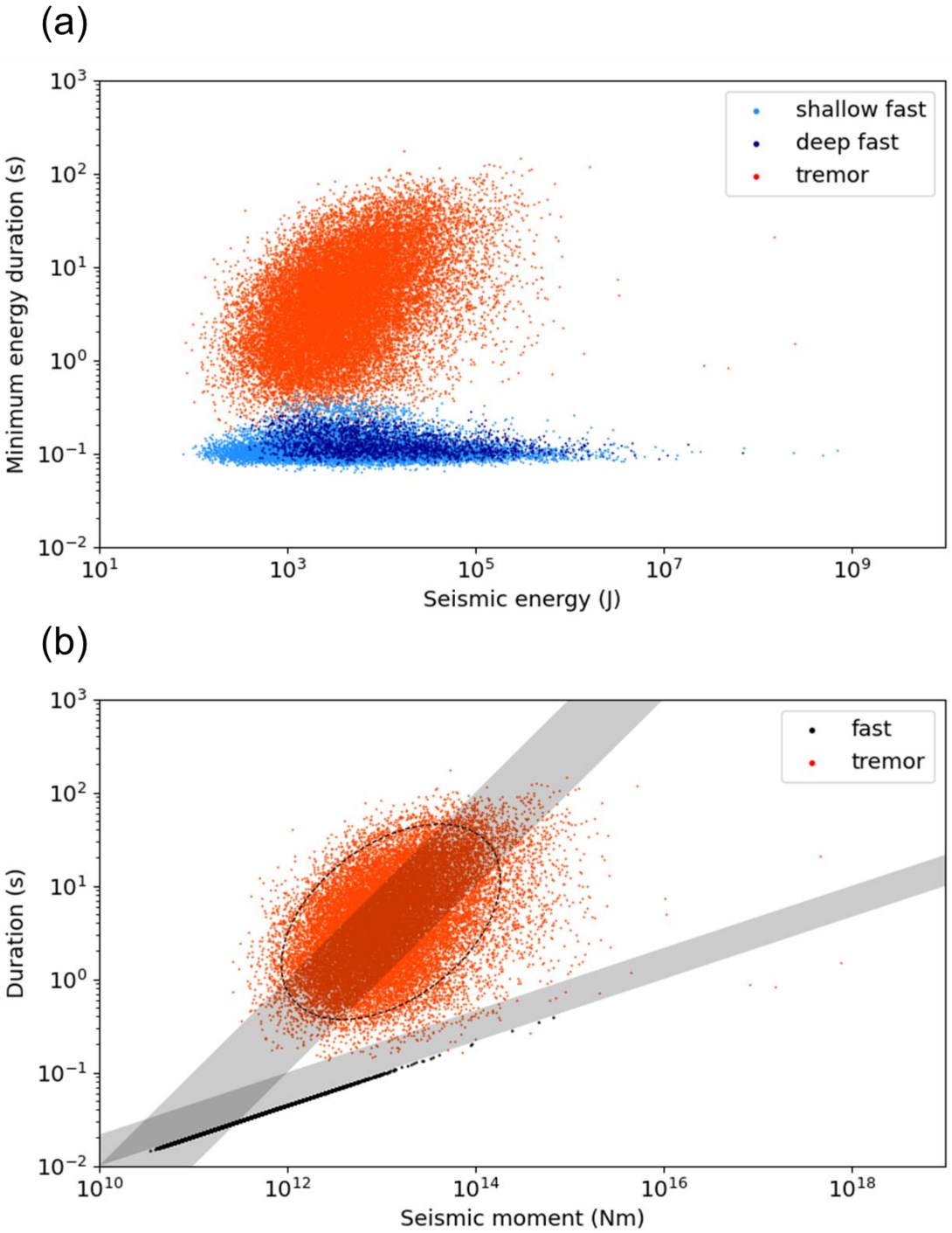

Figure 4. (a) Comparison of observed seismic energy E_s^{obs} and minimum energy duration τ_e. Light and dark blue dots correspond to $C_{shallow}$ and C_{deep}, respectively. Orange dots depict Quality A and B tremors. (b) Comparison of estimated seismic moment M_0 and event duration, where the duration of fast earthquakes is estimated from E_s^{obs} using the omega-square model, whereas that of tremors is τ_e itself. The two gray lines represent $M_0 = \tau^3 \times 10^{15-16}$ for fast earthquakes and $M_0 = \tau \times 10^{12-13}$ for slow earthquakes. The dashed ellipse shows the region containing 95 % of the tremors.

6 Conclusion

We improved the envelope cross-correlation method proposed by Mizuno and Ide (2019) to compile a more comprehensive catalog of tectonic tremors. We introduced a new definition of duration (minimum energy duration) and calculated mean amplitudes at high- and low-frequency ranges. Using these event features, we developed a scheme for compiling an objective tremor catalog using a density-based clustering algorithm and supervised learning. Detected tremors are categorized into Quality A and Quality B tremors, constituting more reliable and more complete catalogs, respectively.

The application of our method to continuous seismograms for western Japan detects 1.7 times more tremors compared with the original method. The spatial distribution of tremors is similar to that of previous results. Comparison with the JMA catalog reveals that the accuracy of our tremor detection exceeds 99 %. Detected tremors have a wide range of durations, from 0.3 to 100 s, encompassing 8,415 events with short durations that were previously rejected by the conventional method. Some of these short-duration events are LFEs that have been manually identified by the JMA. The duration distribution is described well by an exponential law, suggesting the existence of a scale limit in the background physical process.

This study is the first to provide a comprehensive scaling relationship for slow earthquakes, ranging from LFEs with durations of ~0.3 s to tremors with durations of more than 100 s. This relationship bridges the 1–10 s gap, in which seismological observation is difficult due to large microseism noise. Given that the proportionality between seismic energy and seismic moment holds for this scale range, the seismic moment is proportional to the duration, with a proportionality coefficient of approximately 10^{12-13} Nm/s, which is consistent with the relationship suggested for the very wide range of time scales from LFEs to SSEs.

Acknowledgements

This research is supported by JSPS Kakenhi (21H04505), MEXT Kakenhi (21H05200), and Earthquake and Volcano Hazards Observation and Research.

Open Research

The seismic data of Hi-net are available at https://www.hinet.bosai.go.jp/?LANG=en

after obtaining an ID from https://hinetwww11.bosai.go.jp/nied/registration/?LANG=en. The code of seismic event detection by Mizuno and Ide (2019) is available at https://github.com/not522/MizunoIde2019. Our algorithm is implemented using NLopt (Johnson, 2014), GNU Parallel (Tange, 2018), and Scikit-learn (Pedregosa et al., 2018). The figures in this manuscript are prepared using Matplotlib (Hunter, 2007) and GMT (Wessel et al., 2019).

References

Aguiar, A. C., Melbourne, T. I., & Scrivner, C. W. (2009). Moment release rate of Cascadia tremor constrained by GPS. *Journal of Geophysical Research: Solid Earth*, *114*(B7). https://doi.org/10.1029/2008JB005909

Aki, K. (1967). Scaling law of seismic spectrum. *Journal of Geophysical Research (1896-1977)*, *72*(4), 1217–1231. https://doi.org/10.1029/JZ072i004p01217

Aki, K., & Koyanagi, R. (1981). Deep volcanic tremor and magma ascent mechanism under Kilauea, Hawaii. *Journal of Geophysical Research: Solid Earth*, *86*(B8), 7095–7109. https://doi.org/10.1029/JB086iB08p07095

Baba, T., Tanioka, Y., Cummins, P. R., & Uhira, K. (2002). The slip distribution of the 1946 Nankai earthquake estimated from tsunami inversion using a new plate model. *Physics of the Earth and Planetary Interiors*, *132*(1), 59–73. https://doi.org/10.1016/S0031-9201(02)00044-4

Baiesi, M., & Paczuski, M. (2004). Scale-free networks of earthquakes and aftershocks. *Physical Review E*, *69*(6), 066106. https://doi.org/10.1103/PhysRevE.69.066106

Behr, W. M., & Bürgmann, R. (2021). What's down there? The structures, materials and environment of deep-seated slow slip and tremor. *Philosophical Transactions of the Royal Society A: Mathematical, Physical and Engineering Sciences*, *379*(2193), 20200218. https://doi.org/10.1098/rsta.2020.0218

Benoit, J. P., McNutt, S. R., & Barboza, V. (2003). Duration-amplitude distribution of volcanic tremor. *Journal of Geophysical Research: Solid Earth*, *108*(B3). https://doi.org/10.1029/2001JB001520

Beroza, G. C., & Ide, S. (2011). Slow Earthquakes and Nonvolcanic Tremor. *Annual Review of Earth and Planetary Sciences*, *39*(1), 271–296. https://doi.org/10.1146/annurev-earth-040809-152531

Bletery, Q., Thomas, A. M., Hawthorne, J. C., Skarbek, R. M., Rempel, A. W., & Krogstad, R.

D. (2017). Characteristics of secondary slip fronts associated with slow earthquakes in Cascadia. *Earth and Planetary Science Letters*, *463*, 212–220. https://doi.org/10.1016/j.epsl.2017.01.046

Bostock, M. G., Thomas, A. M., Savard, G., Chuang, L., & Rubin, A. M. (2015). Magnitudes and moment-duration scaling of low-frequency earthquakes beneath southern Vancouver Island. *Journal of Geophysical Research: Solid Earth*, *120*(9), 6329–6350. https://doi.org/10.1002/2015JB012195

Box, G. E. P., & Cox, D. R. (1964). An Analysis of Transformations. *Journal of the Royal Statistical Society. Series B (Methodological)*, *26*(2), 211–252.

Campello, R. J. G. B., Moulavi, D., & Sander, J. (2013). Density-Based Clustering Based on Hierarchical Density Estimates. In J. Pei, V. S. Tseng, L. Cao, H. Motoda, & G. Xu (Eds.), *Advances in Knowledge Discovery and Data Mining* (pp. 160–172). Berlin, Heidelberg: Springer. https://doi.org/10.1007/978-3-642-37456-2_14

Chestler, S. R., & Creager, K. C. (2017). Evidence for a scale-limited low-frequency earthquake source process. *Journal of Geophysical Research: Solid Earth*, *122*(4), 3099–3114. https://doi.org/10.1002/2016JB013717

Farge, G., Shapiro, N. M., & Frank, W. B. (2020). Moment-Duration Scaling of Low-Frequency Earthquakes in Guerrero, Mexico. *Journal of Geophysical Research: Solid Earth*, *125*(8), e2019JB019099. https://doi.org/10.1029/2019JB019099

Gomberg, J., Wech, A., Creager, K., Obara, K., & Agnew, D. (2016). Reconsidering earthquake scaling. *Geophysical Research Letters*, *43*(12), 6243–6251. https://doi.org/10.1002/2016GL069967

Gombert, B., & Hawthorne, J. C. (2023). Rapid Tremor Migration During Few Minute-Long Slow Earthquakes in Cascadia. *Journal of Geophysical Research: Solid Earth*, *128*(2), e2022JB025034. https://doi.org/10.1029/2022JB025034

Hiramatsu, Y., Watanabe, T., & Obara, K. (2008). Deep low-frequency tremors as a proxy for slip monitoring at plate interface. *Geophysical Research Letters*, *35*(13). https://doi.org/10.1029/2008GL034342

Hirose, F., Nakajima, J., & Hasegawa, A. (2008). Three-dimensional seismic velocity structure and configuration of the Philippine Sea slab in southwestern Japan estimated by double-difference tomography. *Journal of Geophysical Research: Solid Earth*, *113*(B9). https://doi.org/10.1029/2007JB005274

Hunter, J. D. (2007). Matplotlib: A 2D Graphics Environment. *Computing in Science &*

Engineering, *9*(3), 90–95. https://doi.org/10.1109/MCSE.2007.55

Ide, S. (2010). Striations, duration, migration and tidal response in deep tremor. *Nature*, *466*(7304), 356–359. https://doi.org/10.1038/nature09251

Ide, S., & Beroza, G. C. (2023). Slow earthquake scaling reconsidered as a boundary between distinct modes of rupture propagation. *Proceedings of the National Academy of Sciences*, *120*(32), e2222102120. https://doi.org/10.1073/pnas.2222102120

Ide, S., Beroza, G. C., Shelly, D. R., & Uchide, T. (2007). A scaling law for slow earthquakes. *Nature*, *447*(7140), 76–79. https://doi.org/10.1038/nature05780

Johnson, S. G. (2014). The NLopt nonlinear-optimization package, http://github.com/stevengj/nlopt. Retrieved January 11, 2024, from https://nlopt.readthedocs.io/en/latest/Citing_NLopt/

Madariaga, R. (1976). Dynamics of an Expanding Circular Fault. *Bulletin of the Seismological Society of America*, *66*, 639–666. https://doi.org/10.1785/BSSA0660030639

Maeda, T., & Obara, K. (2009). Spatiotemporal distribution of seismic energy radiation from low-frequency tremor in western Shikoku, Japan. *Journal of Geophysical Research: Solid Earth*, *114*(B10). https://doi.org/10.1029/2008JB006043

Maury, J., Ide, S., Cruz-Atienza, V. M., & Kostoglodov, V. (2018). Spatiotemporal Variations in Slow Earthquakes Along the Mexican Subduction Zone. *Journal of Geophysical Research: Solid Earth*, *123*(2), 1559–1575. https://doi.org/10.1002/2017JB014690

Mizuno, N., & Ide, S. (2019). Development of a modified envelope correlation method based on maximum-likelihood method and application to detecting and locating deep tectonic tremors in western Japan. *Earth, Planets and Space*, *71*(1), 40. https://doi.org/10.1186/s40623-019-1022-x

Moulavi, D., Jaskowiak, P. A., Campello, R. J. G. B., Zimek, A., & Sander, J. (2014). Density-Based Clustering Validation. In *Proceedings of the 2014 SIAM International Conference on Data Mining* (pp. 839–847). Society for Industrial and Applied Mathematics. https://doi.org/10.1137/1.9781611973440.96

Nakajima, J., & Hasegawa, A. (2007). Subduction of the Philippine Sea plate beneath southwestern Japan: Slab geometry and its relationship to arc magmatism. *Journal of Geophysical Research: Solid Earth*, *112*(B8). https://doi.org/10.1029/2006JB004770

Nakajima, J., & Hasegawa, A. (2021). Prevalence of Shallow Low-Frequency Earthquakes in the Continental Crust. *Journal of Geophysical Research: Solid Earth*, *126*(4),

e2020JB021391. https://doi.org/10.1029/2020JB021391

Nishikawa, T., Ide, S., & Nishimura, T. (2023). A review on slow earthquakes in the Japan Trench. *Progress in Earth and Planetary Science*, *10*(1), 1. https://doi.org/10.1186/s40645-022-00528-w

Obara, K. (2002). Nonvolcanic Deep Tremor Associated with Subduction in Southwest Japan. *Science*, *296*(5573), 1679–1681. https://doi.org/10.1126/science.1070378

Obara, K., & Kato, A. (2016). Connecting slow earthquakes to huge earthquakes. *Science*, *353*(6296), 253–257. https://doi.org/10.1126/science.aaf1512

Pedregosa, F., Varoquaux, G., Gramfort, A., Michel, V., Thirion, B., Grisel, O., et al. (2018, June 5). Scikit-learn: Machine Learning in Python (Version 4). arXiv. https://doi.org/10.48550/arXiv.1201.0490

Peterson, J. R. (1993). *Observations and modeling of seismic background noise* (USGS Numbered Series No. 93–322). *Observations and modeling of seismic background noise* (Vol. 93–322). U.S. Geological Survey. https://doi.org/10.3133/ofr93322

Romanet, P., & Ide, S. (2019). Ambient tectonic tremors in Manawatu, Cape Turnagain, Marlborough, and Puysegur, New Zealand. *Earth, Planets and Space*, *71*(1), 59. https://doi.org/10.1186/s40623-019-1039-1

Sit, S., Brudzinski, M., & Kao, H. (2012). Detecting tectonic tremor through frequency scanning at a single station: Application to the Cascadia margin. *Earth and Planetary Science Letters*, *353–354*, 134–144. https://doi.org/10.1016/j.epsl.2012.08.002

Supino, M., Poiata, N., Festa, G., Vilotte, J. P., Satriano, C., & Obara, K. (2020). Self-similarity of low-frequency earthquakes. *Scientific Reports*, *10*(1), 6523. https://doi.org/10.1038/s41598-020-63584-6

Tange, O. (2018). *GNU Parallel 2018*. Ole Tange. https://doi.org/10.5281/zenodo.1146014

Toh, A., Capdeville, Y., Chi, W.-C., & Ide, S. (2023). Strongly Scattering Medium Along Slow Earthquake Fault Zones Based on New Observations of Short-Duration Tremors. *Geophysical Research Letters*, *50*(8), e2022GL101851. https://doi.org/10.1029/2022GL101851

Tozer, B., Sandwell, D. T., Smith, W. H. F., Olson, C., Beale, J. R., & Wessel, P. (2019). Global Bathymetry and Topography at 15 Arc Sec: SRTM15+. *Earth and Space Science*, *6*(10), 1847–1864. https://doi.org/10.1029/2019EA000658

Ueno, H., Hatakeyama, S., Aketagawa, T., Funasaki, J., & Hamada, N. (2002). Improvement of hypocenter determination procedures in the Japan Meteorological Agency. *Quater.*

J. Seismol., *65*, 123–134.

Watanabe, T., Hiramatsu, Y., & Obara, K. (2007). Scaling relationship between the duration and the amplitude of non-volcanic deep low-frequency tremors. *Geophysical Research Letters*, *34*(7). https://doi.org/10.1029/2007GL029391

Wech, A. G., & Creager, K. C. (2007). Cascadia tremor polarization evidence for plate interface slip. *Geophysical Research Letters*, *34*(22). https://doi.org/10.1029/2007GL031167

Wech, A. G., & Creager, K. C. (2008). Automated detection and location of Cascadia tremor. *Geophysical Research Letters*, *35*(20). https://doi.org/10.1029/2008GL035458

Wech, A. G., Creager, K. C., Houston, H., & Vidale, J. E. (2010). An earthquake-like magnitude-frequency distribution of slow slip in northern Cascadia. *Geophysical Research Letters*, *37*(22). https://doi.org/10.1029/2010GL044881

Wessel, P., Luis, J. F., Uieda, L., Scharroo, R., Wobbe, F., Smith, W. H. F., & Tian, D. (2019). The Generic Mapping Tools Version 6. *Geochemistry, Geophysics, Geosystems*, *20*(11), 5556–5564. https://doi.org/10.1029/2019GC008515

Yabe, S., & Ide, S. (2014). Spatial distribution of seismic energy rate of tectonic tremors in subduction zones. *Journal of Geophysical Research: Solid Earth*, *119*(11), 8171–8185. https://doi.org/10.1002/2014JB011383

Zaliapin, I., & Ben-Zion, Y. (2013). Earthquake clusters in southern California I: Identification and stability. *Journal of Geophysical Research: Solid Earth*, *118*(6), 2847–2864. https://doi.org/10.1002/jgrb.50179

Zaliapin, I., Gabrielov, A., Keilis-Borok, V., & Wong, H. (2008). Clustering Analysis of Seismicity and Aftershock Identification. *Physical Review Letters*, *101*(1), 018501. https://doi.org/10.1103/PhysRevLett.101.018501